



# Prednisolone rescues Duchenne muscular dystrophy phenotypes in human pluripotent stem cell–derived skeletal muscle in vitro

Ziad Al Tanoury<sup>a,b,c,d,1</sup>, John F. Zimmerman<sup>d,e,1</sup>, Jyoti Rao<sup>b,c,d,1</sup>, Daniel Sieiro<sup>b,c,d,1</sup>, Harold M. McNamara<sup>f,g,1</sup>, Thomas Cherrier<sup>a,1</sup>, Alejandra Rodríguez-delaRosa<sup>b,c,d</sup>, Aurore Hick-Colin<sup>h</sup>, Fanny Bousson<sup>h</sup>, Charlotte Fugier-Schmucker<sup>h</sup>, Fabio Marchiano<sup>i</sup>, Bianca Habermann<sup>i</sup>, Jérôme Chal<sup>a,b,c,d</sup>, Alexander P. Nesmith<sup>d,e</sup>, Svetlana Gapon<sup>b</sup>, Erica Wagner<sup>b</sup>, Vandana A. Gupta<sup>j</sup>, Rhonda Bassel-Duby<sup>k,l,m</sup>, Eric N. Olson<sup>k,l,m</sup>, Adam E. Cohen<sup>f,g</sup>, Kevin Kit Parker<sup>d,e</sup>, and Olivier Pourquie<sup>a,b,c,d,z</sup>

<sup>a</sup>Institut de Génétique et de Biologie Moléculaire et Cellulaire, CNRS UMR 7104, INSERM U964, Université de Strasbourg, 67411 Illkirch Graffenstaden, France; <sup>b</sup>Department of Pathology, Brigham and Women's Hospital, Boston, MA 02115; <sup>c</sup>Department of Genetics, Harvard Medical School, Boston, MA 02115; <sup>d</sup>Harvard Stem Cell Institute, Harvard University, Boston, MA 02138; <sup>e</sup>Disease Biophysics Group, Wyss Institute for Biologically Inspired Engineering, Harvard John A. Paulson School of Engineering and Applied Sciences, Boston, MA 02134; <sup>f</sup>Department of Chemistry and Chemical Biology, Harvard University, Cambridge, MA 02138; <sup>g</sup>Department of Physics, Harvard University, Cambridge, MA 02138; <sup>h</sup>Anagenesis Biotechnologies, 67400 Illkirch Graffenstaden, France; <sup>i</sup>Aix-Marseille University, CNRS, Institut de Biologie du Développement de Marseille UMR 7288, The Turing Center for Living Systems, 13009 Marseille, France; <sup>j</sup>Division of Genetics, Brigham and Women's Hospital, Harvard Medical School, Boston, MA 02115; <sup>k</sup>Department of Molecular Biology, University of Texas Southwestern Medical Center, Dallas, TX 75390; <sup>l</sup>Hamon Center for Regenerative Science and Medicine, University of Texas Southwestern Medical Center, Dallas, TX 75390; and <sup>m</sup>Senator Paul D. Wellstone Muscular Dystrophy Cooperative Research Center, University of Texas Southwestern Medical Center, Dallas, TX 75390

Contributed by Olivier Pourquie, June 2, 2021 (sent for review November 3, 2020); reviewed by Pura Muñoz-Cánoves and Frédéric Relaix

**Duchenne muscular dystrophy (DMD) is a devastating genetic disease leading to degeneration of skeletal muscles and premature death. How dystrophin absence leads to muscle wasting remains unclear. Here, we describe an optimized protocol to differentiate human induced pluripotent stem cells (iPSC) to a late myogenic stage. This allows us to recapitulate classical DMD phenotypes (mislocalization of proteins of the dystrophin-associated glycoprotein complex, increased fusion, myofiber branching, force contraction defects, and calcium hyperactivation) in isogenic DMD-mutant iPSC lines in vitro. Treatment of the myogenic cultures with prednisolone (the standard of care for DMD) can dramatically rescue force contraction, fusion, and branching defects in DMD iPSC lines. This argues that prednisolone acts directly on myofibers, challenging the largely prevalent view that its beneficial effects are caused by antiinflammatory properties. Our work introduces a human in vitro model to study the onset of DMD pathology and test novel therapeutic approaches.**

pluripotent stem cell | Duchenne muscular dystrophy | dystrophin | myopathy | myogenesis

**D**uchenne muscular dystrophy (DMD) is an X-linked muscular dystrophy (affecting 1 in 5,000 boys) caused by mutations in the dystrophin gene (*DMD*) (1). There is currently no cure for the disease and the only available treatment is glucocorticoids, which can prolong the ambulatory phase (2). The dystrophin protein plays a key role in organizing a molecular complex (dystrophin-associated glycoprotein complex [DGC]) spanning the sarcolemma at the level of costameres and linking the actin cytoskeleton to laminin and extracellular matrix. In DMD patients fibers are more sensitive to mechanical stress and experience formation of membrane tears upon muscle contraction (3). DMD mutant myofibers exhibit abnormal calcium homeostasis, displaying higher resting calcium levels (4). The DGC also acts as an important scaffold necessary for the function of several signaling proteins such as nitric oxide synthase (nNOS) (5). In the early stages of the disease, the degeneration of muscle fibers stimulates regeneration of new fibers from satellite cells, a physiological response that counterbalances fiber loss and maintains a normal muscle function. This increased generation of fibers is accompanied by structural defects such as branching of the newly generated fibers, possibly resulting from fusion defects of the regenerating cells (6, 7). As the disease progresses, satellite cell regeneration

capacity decreases, leading to tissue fibrosis. This myofiber degeneration and fibrosis are considered to be largely responsible for the decrease in muscle strength observed in patients. There is also evidence suggesting intrinsic contractile dysfunction in zebrafish, mice, and dogs lacking dystrophin (8–10). Due to difficulties in accessing patient muscle fibers, evidence for such contractile defects and their cause and significance in the progression of the human diseased phenotypes has remained very limited (11).

## Significance

**Duchenne muscular dystrophy (DMD) is a devastating disease caused by mutation in the X-linked dystrophin gene, resulting in skeletal muscle loss and patient premature death. Here, we present an improved protocol for the differentiation of human pluripotent stem cells to the skeletal muscle lineage. Using this protocol for the differentiation of human isogenic-induced pluripotent stem cells lacking the DMD gene, we can reproduce several features of the pathology including mislocalization of proteins of the dystrophin-associated complex, increased fiber branching, contraction defects, and calcium signaling hyperactivity. Several of these defects can be rescued in part in vitro by treating cells with prednisolone, the standard of care for DMD patients, supporting direct action of this drug on the diseased fibers.**

Author contributions: O.P. designed research; Z.A.T., J.F.Z., J.R., D.S., H.M.M., T.C., A.R.-d.I.R., A.H.-C., F.B., C.F.-S., J.C., A.P.N., S.G., and E.W. performed research; Z.A.T., J.F.Z., J.R., D.S., H.M.M., A.R.-d.I.R., A.H.-C., F.M., B.H., and V.A.G. analyzed data; O.P. wrote the paper; R.B.-D. and E.N.O. provided the Duchenne muscular dystrophy patient iPSC line and its CRISPR-corrected version; A.E.C. supervised the calcium experiments; K.K.P. supervised the force contraction experiments; and O.P. supervised the project.

Reviewers: P.M.-C., Universitat Pompeu Fabra; and F.R., Université Paris-Est Créteil.

Competing interest statement: O.P. and J.C. are founders and shareholders of Anagenesis Biotechnologies. R.B.-D. and E.N.O. are consultants for Exonics Therapeutics/Vertex Genetic Therapies. A.E.C. is a cofounder and Scientific Advisory Board member of Q-State Biosciences. K.K.P. is a shareholder of Emulate.

Published under the [PNAS license](https://www.pnas.org/lookup/suppl/doi:10.1073/pnas.2022960118/-DCSupplemental).

<sup>1</sup>Z.A.T., J.F.Z., J.R., D.S., H.M.M., and T.C. contributed equally to this work.

<sup>2</sup>To whom correspondence may be addressed. Email: [pourquie@genetics.med.harvard.edu](mailto:pourquie@genetics.med.harvard.edu).

This article contains supporting information online at <https://www.pnas.org/lookup/suppl/doi:10.1073/pnas.2022960118/-DCSupplemental>.

Published July 6, 2021.

Much of the research on the etiology of DMD as well as preclinical tests for the validation of DMD therapeutic strategies have been carried out in the *mdx* mouse, a spontaneous dystrophin mutant (12). In the *mdx* mouse myofibers, defects such as branching and misalignment are detected as early as embryonic day 13.5 at the beginning of the fetal period (13). A significant limitation of the *mdx* model is that the dystrophy is much less severe and only partly phenocopies the human disease (12). There is therefore a critical need for a better preclinical model in which the disease can be recapitulated with human myofibers. The recent development of protocols to differentiate human pluripotent stem cells such as induced pluripotent stem cells (iPSCs) to skeletal myofibers in vitro (14) now offers the possibility to generate DMD models better reflecting the physiology of human cells. Several studies describing the establishment of DMD patient iPSC lines and their differentiation to skeletal muscles have been reported (15). However, only a limited set of relevant phenotypes have been analyzed and the impact on skeletal muscle contractility has not been investigated.

Here we describe an optimized myogenic differentiation protocol resulting in significantly improved myofiber maturation from human pluripotent cells in vitro, as shown by the expression of all fast myosin isoforms. Using this optimized protocol, we show that muscle fibers derived from two human isogenic iPSC cell lines carrying different DMD mutations engineered in a healthy iPSC line recapitulate most hallmarks of the DMD phenotype compared with the parental line. These include mislocalization of DGC proteins such as nNOS, branching/fusion defects, and calcium signaling hyperactivation. We also demonstrate that skeletal myofibers derived from the DMD mutant lines exhibit defective contractions, strongly supporting the notion that an intrinsic contractility defect also contributes to the muscle weakness phenotype in DMD patients. Remarkably, this contraction defect can be largely rescued by prednisolone treatment, indicating that the drug directly acts on mutant fibers. Finally, these DMD phenotypes are also observed in an iPSC line derived from a DMD patient differentiated using the optimized protocol and they are rescued when restoring the *DMD* coding frame using CRISPR-Cas9, demonstrating their specificity. Thus, our work provides an in vitro platform to study the etiology of DMD in human myofibers. Our human DMD in vitro model will allow for exploration of the early contraction and branching defects caused by absence of dystrophin at the origin of the pathology and offers a platform for preclinical testing of candidate therapies for this devastating disease.

## Results

### Optimization of the Maturation of Human iPSC-Derived Muscle Fibers.

We have developed a two-step muscle differentiation protocol for human pluripotent stem cells which first recapitulates the early stages of paraxial mesoderm differentiation followed by myogenesis in vitro (Fig. 1A) (16, 17). During the first step (primary differentiation), cells are cultured for 3 to 4 wk in a series of different media, resulting in the formation of long striated myofibers interspersed with PAX7-positive myogenic precursors (17). To monitor progress through myogenic differentiation in these conditions, we performed RNA sequencing (RNA-seq) of the cultures at days 0, 8, 16, 24, and 32 of differentiation (Fig. 1B) (18). We observed a sequence of expression of myogenic markers starting with *PAX3* at day 8 followed by *PAX7* at day 16. At day 16, we first detected *MYF5*, *MYOG*, and *MYOD1*, which peaked later between day 24 and 32 when the marker for fetal (secondary) myogenesis *NFIX* was strongly expressed (19). Messenger RNAs (mRNAs) for sarcomeric proteins such as  $\alpha$ -actinin (*ACTN2*) or titin (*TTN*) were first detected at day 16 and peaked at day 32. At day 32 we also detected expression of both embryonic (*CHRNA2*) and adult (*CHRNA1*) subunits of the acetylcholine receptor. Overall,

these data suggest that the primary differentiation protocol recapitulates embryonic and fetal myogenesis in vitro.

In the second step, which can be performed after ~20 to 30 d in vitro, the myogenic cultures are dissociated and replated in proliferation medium (SKGM), resulting in enrichment in myogenic precursors (Fig. 1A) (17). After 1 to 2 d, as the replated cells reach confluence, the basal differentiation medium is switched to a medium containing the Wnt agonist CHIR and KSR (Knockout Serum Replacement). This results in cultures highly enriched for long striated myofibers after 7 d (Fig. 1F, I, and L). We next analyzed the effect of supplementing the basal medium with a transforming growth factor type  $\beta$  (TGF- $\beta$ ) inhibitor (SB-431542) previously reported to enhance fusion efficiency of muscle fibers (20, 21). When differentiated for 1 wk in KSR/CHIR (KC) or in KSR/CHIR/TGF- $\beta$  inhibitor (KCTi) media, the replated cells elongated and rapidly acquired a myogenic phenotype, developing into multinucleated muscle fibers (Fig. 1G, J, and M). During human fetal development, a burst of glucocorticoid signaling is observed around 7 to 14 wk, when fetal myogenesis is ongoing (22). To recreate conditions similar to that experienced by the developing human fetus, we treated the replated cultures differentiating in KCTi with prednisolone (KSR/CHIR/TGF $\beta$ i/prednisolone [KCTiP]), a synthetic glucocorticoid hormone previously shown to promote myogenic differentiation in wild-type (WT) and *mdx* primary myoblast cultures (23). Even though expected myogenic markers were expressed in cultures differentiated in KC and KCTi, we noted a very significant improvement of the morphology of cultures treated with KCTiP with more organized myofibrils (Fig. 1H, K, and N and *SI Appendix, Fig. S1 A–R*).

We next examined the expression of myosin heavy chain isoforms mRNAs which are sequentially activated during skeletal muscle development (24). Embryonic myosin heavy chain (*MYH3*) was strongly expressed at day 16 of primary differentiation, while a weak expression of neonatal myosin (*MYH8*) and slow myosin (*MYH7*) was observed at this stage (Fig. 1B). Expression of *MYH8* and *MYH7* strongly increased at day 32 in the cultures. During primary differentiation we only detected low levels of expression of the fast myosin IIX (*MYH1*), IIA (*MYH2*), and IIB (*MYH4*), which are respectively first expressed during fetal, late fetal, and early postnatal stages (24). We also performed RNA-seq analysis of the secondary cultures differentiated following replating in KC and KCTi for 1 or 2 wk and compared them with the nondifferentiated myogenic progenitors grown in SKGM and to primary differentiation (Fig. 1A and B) (18). When compared with primary differentiation and to KC medium, KCTi induced a higher level of expression of the fast myosins *MYH1* and *MYH2* and *MYH4*. RNA-seq analysis of cultures in KCTiP show a further increased expression of *MYH1*, *MYH2*, *MYH4*, and *MYH8* compared with cultures differentiated in KCTi only (Fig. 1B). *MYH1*, *MYH2*, and *MYH8* up-regulation in KCTiP was validated by reverse transcription qPCR (Fig. 1C–E). Additionally, transmission electron microscopy was performed in cultures differentiated in KC, KCTi, and KCTiP. Fibers generated in KCTi medium appeared thicker with better-organized sarcomeres compared with the KC medium (Fig. 1O–P). Cultures differentiated in KCTiP show a trend toward a higher percentage of myofibers with mature sarcomeres, defined by the presence of Z-bodies, H zones, and actin–myosin assemblies, compared with KCTi or KC (Fig. 1R). Also, KCTiP-derived mature sarcomeres show longer Z-bodies/lines than those obtained with KC or KCTi (Fig. 1Q and S), suggesting more mature sarcomeres. Thus, exposing differentiating human iPSC cultures to glucocorticoids promotes the maturation of skeletal myofibers.

### Generation and Differentiation of Isogenic DMD Mutant iPSC Cell Lines.

We used CRISPR-Cas9-mediated gene editing to establish isogenic cell lines in which DMD mutations were engineered into the WT human iPSC line NCRM1 (25). We engineered a full deletion of exon 52 (hereafter named DMDI) and a point mutation

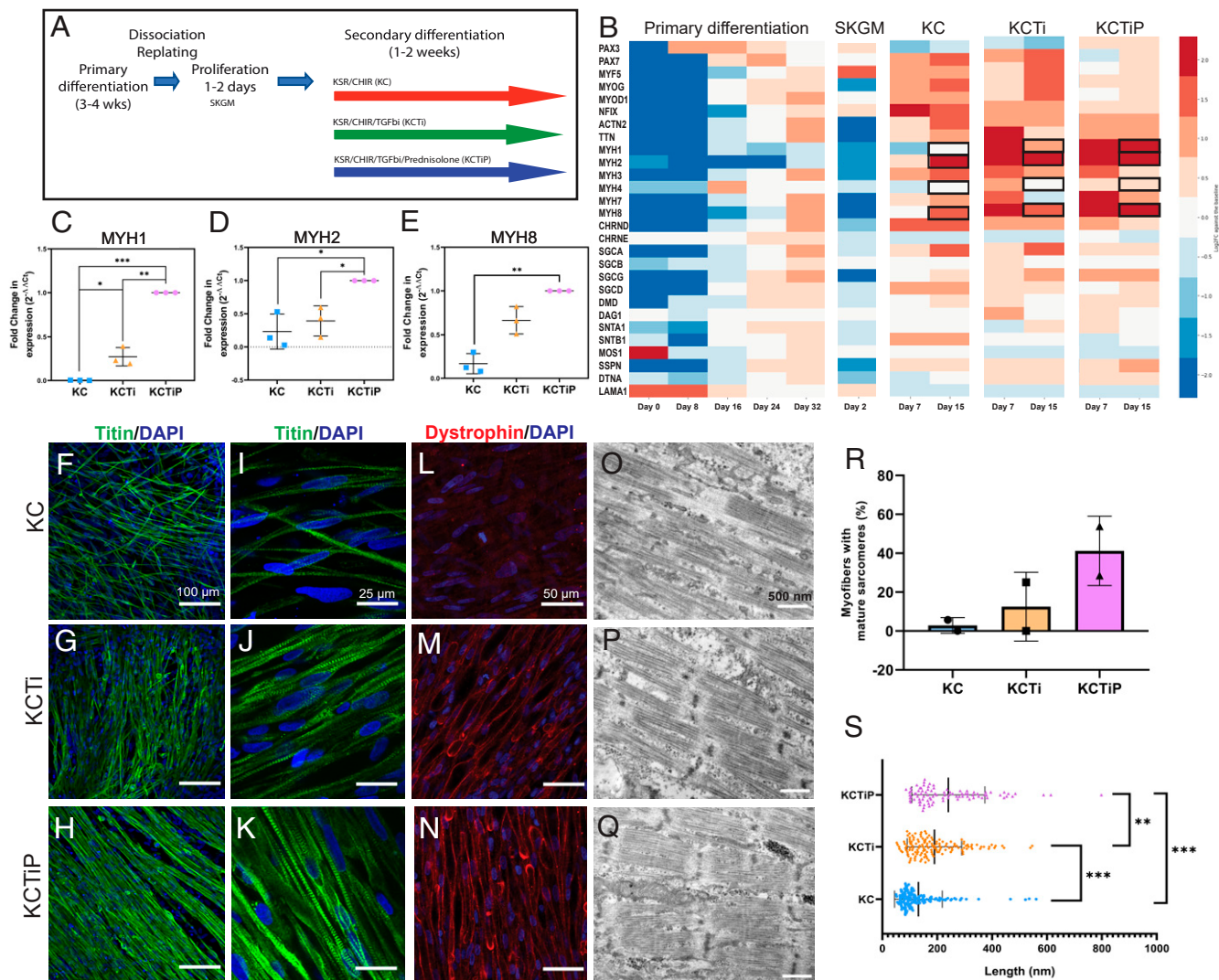


**Fig. 1.** Generation and maturation of iPSC-derived myofibers. (A) Schematic description of the two-step myogenic differentiation protocol. (B) RNA-seq analysis of the myogenic differentiation of WT human iPSCs in vitro. Heat map showing expression levels of selected myogenic markers at different time points during primary differentiation, proliferation in SKGM after replating, and secondary differentiation in KC, KCTi, or KCTiP media. (C–E) Fold changes of mRNA expression of *MYH1* (C), *MYH2* (D), and *MYH8* (E) in secondary cultures differentiated for 1 wk in KC, KCTi, and KCTiP ( $n = 3$ , paired  $t$  test,  $*P < 0.05$ ,  $**P < 0.01$ ,  $***P < 0.001$ ). Bars show mean  $\pm$  SD. (F–K) Titin antibody staining of secondary cultures differentiated for 1 wk in KC (F and I), KCTi (G and J), and KCTiP (H and K) media. (Scale bars: 100  $\mu$ m in F–H and 25  $\mu$ m in I–K.) (L–N) Dystrophin immunocytochemistry analysis following secondary differentiation for 1 wk in KC (L), KCTi (M), and KCTiP (N) media. (Scale bars: 50  $\mu$ m.) (O–Q) Transmission electron microscopy images of secondary cultures differentiated for 10 d in KC (O), KCTi (P), and KCTiP (Q). (Scale bars: 500 nm.) (R) Percentage of myofibers with mature sarcomeres identified by transmission electron microscopy of secondary cultures differentiated for 10 d in KC, KCTi, and KCTiP. Bars show mean  $\pm$  SD ( $n = 2$ ). (S) Length of Z-bodies/lines (nanometers) identified by transmission electron microscopy of secondary cultures differentiated for 10 d in KC, KCTi, and KCTiP. Bars show mean  $\pm$  SD ( $n = 2$ , one-way ANOVA followed by Tukey's multiple comparisons test, ANOVA  $P$  value  $< 0.0001$ ,  $**P < 0.01$ ,  $***P < 0.001$ ).

introducing a stop codon in exon 52 (named DMDII). We could not detect any dystrophin protein by Western blot and immunohistochemistry in myofibers derived from the two mutant lines compared with the parental WT line (Fig. 2A–D). To compare the myogenic potential of the DMD cell lines, we performed immunofluorescence analysis for MYOG after 2 d of secondary differentiation in SKGM medium (Fig. 2E). We observed a significant decrease in the number of MYOG-positive cells in the two DMD lines, suggesting that DMD mutation reduces the myogenic capacity of the cells (Fig. 2F). The number of PAX7 cells was also significantly reduced in one of the DMD cell lines (Fig. 2G). Upon differentiation in KCTiP medium for 1 wk we did not observe striking differences when comparing the expression of desmin, titin, and  $\alpha$ -actinin proteins between skeletal muscle fibers formed from the parental WT cells and the two DMD mutant lines (Fig. 2H–J).

Next, we used RNA-seq to compare the transcriptome of myogenic cultures of the two mutant lines with the parental WT line after SKGM amplification and differentiation for 1 wk in KC medium; 742 genes were down-regulated while 915 genes were up-regulated in both DMD lines with a fold change  $>2$  and a false discovery rate  $<0.01$ , when compared with the parental WT cells (Fig. 2N) (18). Gene Ontology (GO) analysis of the differentially expressed genes revealed that down-regulated genes were primarily enriched in GO terms related to muscle including “striated muscle contraction” or “positive regulation of skeletal muscle development” as well as “regulation of protein kinase B signaling” (Dataset S1 and SI Appendix, Fig. S2J). Transcription factors found in these categories included MYOD1, MYF6, MYOG, and MEF2C (Dataset S1). GO terms primarily enriched in the up-regulated genes in DMD cultures included “collagen binding,” “cytokine-activity,”

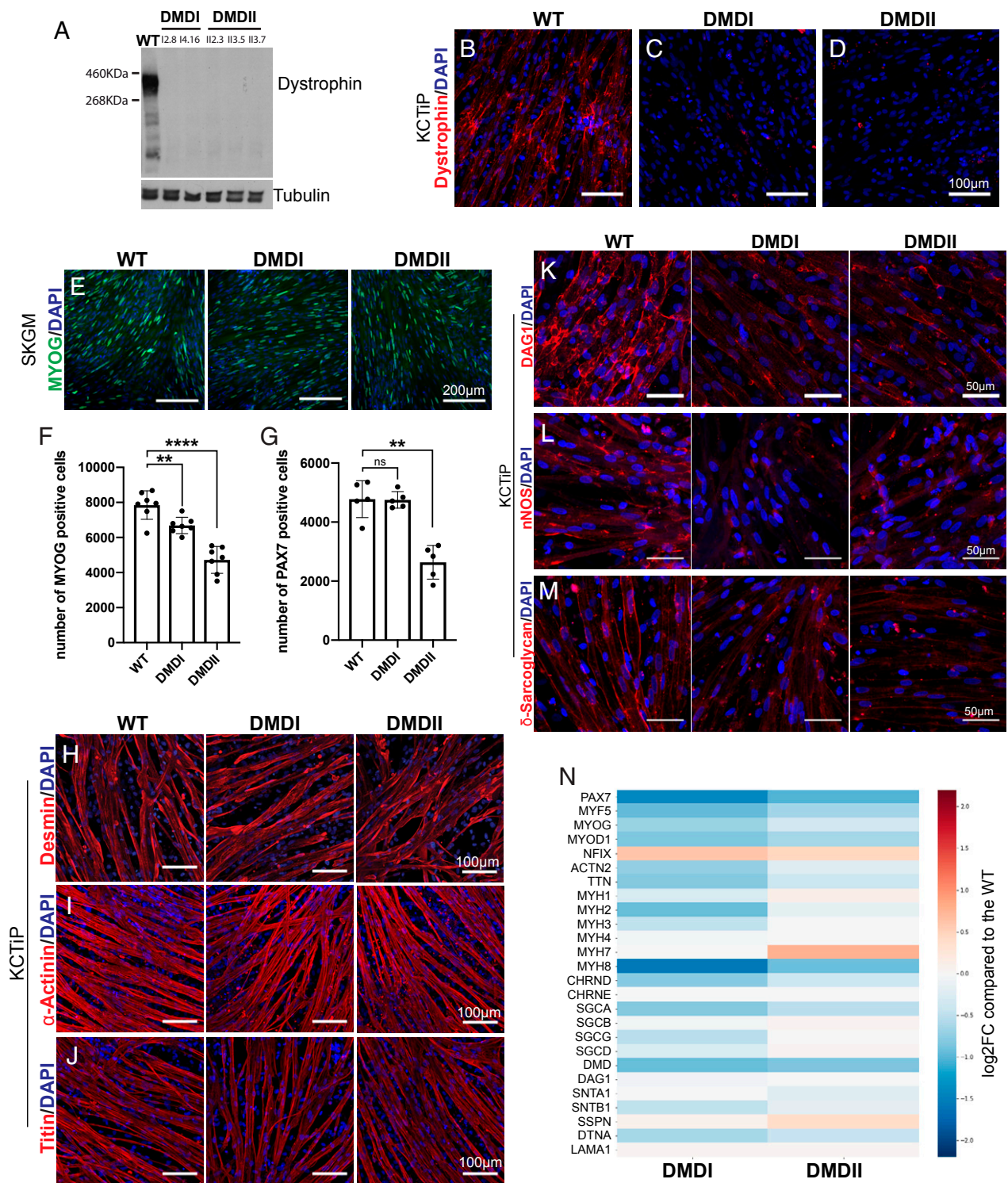


**Fig. 2.** Characterization of isogenic DMD mutant human iPSC lines. (A) Western blot analysis with an anti-dystrophin antibody in two independent clones of the exon 52 deletion mutant (DMDI) and the exon 52-point mutation mutant (DMDII). (Bottom) Tubulin loading control. (B–D) Dystrophin expression detected by immunocytochemistry in WT (B), DMDI (C), and DMDII (D) mutant lines after secondary differentiation for 1 wk in KCTiP medium. (Scale bars: 100  $\mu$ m.) (E) Immunocytochemistry analysis of myogenic precursors using myogenin (MYOG) antibody after 2 d of secondary differentiation in SKGM medium in WT (Left), DMDI (Middle), and DMDII (Right) mutant lines. (Scale bars: 200  $\mu$ m.) (F) Quantification of MYOG-positive cells in myogenic cultures of WT and DMD lines after 2 d of differentiation in SKGM medium ( $n = 7$ , paired  $t$  test,  $***P < 0.01$ ,  $****P < 0.0001$ ). Bars show mean  $\pm$  SD. (G) Quantification of PAX7-positive cells in myogenic cultures of WT and DMD lines after 2 d of differentiation in SKGM medium ( $n = 7$ , paired  $t$  test,  $***P < 0.01$ ; ns, not significant). Bars show mean  $\pm$  SD. (H–J) Immunocytochemistry analysis of WT (Left), DMDI (Middle), and DMDII (Right) lines after secondary differentiation in KCTiP medium for 1 wk. (H) Desmin, (I)  $\alpha$ -actinin, (J) titin (TTN). (Scale bars: 100  $\mu$ m.) (K–M) Immunocytochemistry analysis of WT (Left), DMDI (Middle), and DMDII (Right) lines after secondary differentiation in KCTiP medium for 1 wk. (K) DAG1, (L) nNOS, (M) Delta-sarcoglycan. (Scale bars: 50  $\mu$ m.) (N) RNA-seq analysis of the myogenic differentiation of WT and DMDI and DMDII mutant lines in vitro. Heat map showing expression levels of selected myogenic markers after 1 wk of secondary differentiation in KC medium.

and “transforming growth factor beta receptor binding,” which are in line with the inflammation and fibrosis detected in patients (Dataset S1 and *SI Appendix*, Fig. S2K).

**Mislocalization of Proteins of the DGC in DMD Mutant iPSC Lines.** When parental WT cells were differentiated in KCTiP medium, muscle fibers strongly expressed dystrophin compared with cells cultured in KC or KCTi conditions (Fig. 1 *L–N* and *SI Appendix*, Fig. S2 *A–C*). Moreover, stronger expression of the components of the DGC complex dystroglycan (DAG1) and delta-sarcoglycan was also detected when prednisolone was present in the differentiation medium (*SI Appendix*, Fig. S2 *D–I*). In both DMD mutant lines the DGC proteins nNOS, DAG1, and delta-sarcoglycan were largely absent from the sarcolemma of the myofibers, where they are localized in the parental WT line (Fig. 2 *K–M*). Overall, proteins of the DGC were mislocalized and down-regulated in DMD mutant fibers whereas other membrane-associated proteins such as NCAM1 were not affected (*SI Appendix*, Fig. S3 *A–C*). Therefore, misexpression of DGC proteins reminiscent of the phenotype of DMD patients (5, 26) is observed in DMD skeletal myofibers differentiated in vitro in KCTiP medium.

**Increased Branching and Fusion of Differentiated Dystrophin-Deficient Fibers.** To test whether human DMD fibers generated in vitro exhibit a branching phenotype, myogenic cultures from the two DMD isogenic lines and from the parental WT line were dissociated at 3 wk and replated. After 24 h, progenitors were transfected at low efficiency with membrane green fluorescent protein (GFP) and nuclear mCherry constructs. This allowed us to permanently mark isolated myofibers within the population and then to quantify the number of branching points as well as nuclei within individual fibers. After 1 wk of differentiation in KC medium, fibers with no branches were observed in 77% of cases, with an average of 0.35 branching points per fiber for the entire WT population (Fig. 3 *A, J, and K*). In contrast, in DMD-derived fibers an average of 0.59 branching points per fiber were observed for both mutant lines, while around 65% and 62% of fibers remained unbranched for DMDI and DMDII, respectively (Fig. 3 *A–C, J, and K*). When fibers were differentiated in the presence of TGF- $\beta$  inhibitor (KCTi), a markedly significant increase in branching points was observed when compared with KC medium (Fig. 3 *D–F, J, and K*). WT fibers differentiated in KCTi contained an average of 0.94 branching points, with more than half of the fibers (53.2%) being bifurcated at least once. Dystrophin-deficient fibers averaged a significantly higher number of branching points when compared with WT cells (1.42 and 1.25 for DMDI and DMDII, respectively) in KCTi. We then investigated the effect of prednisolone on myofiber branching. WT fibers grown in KCTiP medium contained no branching points in 79% of cases, a proportion higher than those of WT fibers grown in KCTi medium (Fig. 3 *G–K*). Interestingly, dystrophin-deficient fibers differentiated in KCTiP also showed fewer branching points than those grown in KCTi media, although they maintained a significantly higher number of branches when compared with WT (compare Fig. 3 *D–F* and *G–I*).

We also investigated how the absence of dystrophin impacts the fusion of myocytes. Nuclei labeled by mCherry were counted in isolated fibers in cultures of WT and DMD mutant cells differentiated in KC, KCTi, or KCTiP. In all three different conditions we observed a significant increase in the number of nuclei in the DMD mutants compared with WT fibers (Fig. 3*L*).

To confirm the specificity of the branching and fusion defects in a different genetic background we used a human patient-derived iPSC line harboring an intronic point mutation in intron 47 of the DMD gene (TX1-Unc) and an isogenic line in which the dystrophin coding frame was restored by CRISPR-Cas9 editing (TX1-Cor) (27). Both lines could differentiate efficiently into myofibers expressing sarcomeric proteins in KCTi and KCTiP (*SI Appendix*, Fig. S4 *A–H*). No expression of dystrophin and down-regulation of DAG1

was observed in the TX1-Unc line while expression of these proteins in the TX1-Cor line was similar to WT (*SI Appendix*, Fig. S4 *A, B, G, and H*). The number of branching points and the number of nuclei per fiber was significantly higher in the uncorrected TX1-Unc line in KCTi than in the corrected line (Fig. 3 *M–O*). Remarkably, the number of branching points and of nuclei per fiber could be reduced in both lines by prednisolone treatment (Fig. 3 *M–O*). Strikingly, prednisolone treatment rescued the branching phenotype in the patient iPSC line to the level of the corrected line treated or not with prednisolone (Fig. 3*M*). Thus, our data show that absence of dystrophin leads to an increase in myofiber branching and fusion in three different DMD mutant lines in various differentiation conditions. Remarkably, excessive branching and fusion can be reduced by treating the differentiating cultures with prednisolone.

**Force Contraction Defects Displayed in Dystrophin-Deficient iPSC-Derived Fibers.** To measure the impact of loss of dystrophin on force contraction we engineered contractile myogenic tissues from the WT and DMD mutant lines (Fig. 4*A*) (17, 28). Myogenic cultures of the WT and the DMDI and DMDII mutant iPSC lines were dissociated and seeded onto thin elastomeric gelatin substrates, which were micromolded with line patterns to promote cell alignment (*SI Appendix*, Fig. S5). The replated cells were first cultured for 1 to 2 d in SKGM until they reached confluence and then were differentiated for a week in KCTi medium. In these conditions, myocytes self-organized into continuous multinucleated myofibers, forming muscular thin films (MTFs) with an average myofiber thickness of  $\sim 15 \mu\text{m}$  (Fig. 4 *A–D* and *SI Appendix*, Fig. S6). Immunofluorescence staining of  $\alpha$ -actinin revealed highly aligned sarcomeres in both WT and DMD mutant muscle fibers (Fig. 4 *B–D*).

Muscle constructs were field stimulated using a frequency sweep over 2 to 99 Hz, transitioning between twitch stresses to tetanic contractions. Film deformation was recorded using a stereomicroscope (Fig. 4 *E–G*) and changes in tissue radius,  $r$ , were mapped to contractile stresses. For WT cultures, greater stimulation frequencies lead to increased sustained contractile stresses between 1,000 and 2,000 Pa (Fig. 4*H*). For DMDI and DMDII, increases in stimulation frequency produced only a mild, non-statistically significant increase in contractile stress between 500 and 900 Pa (Fig. 4 *I and J*). For WT cells, stimulation at 99 Hz yielded an approximate specific tensile strength of  $180 \pm 82 \text{ kPa}$ , which is on par with human in vivo muscle measurements (29). Thus, the DMD cell lines showed overall lower contractile stresses and a minimal force–frequency response as compared with WT muscle differentiated in vitro (Fig. 4*K*).

DMDI and DMDII cultures were next differentiated in the presence of prednisolone in KCTiP medium (*SI Appendix*, Fig. S7). After 1 wk, DMD-derived muscle fibers showed a restored contractile function, yielding positive force–frequency relationships with contractile stresses between 1,000 and 2,000 Pa and 850 and 1,400 Pa for DMDII and DMDI, respectively (Fig. 4 *E–G* and *L–N*). These levels were comparable to those of control WT cantilevers, cultured with or without prednisolone (Fig. 4*L* and *Movie S1*).

Additionally, we compared force contraction between the TX1-Unc and TX1-Cor isogenic pair. MTFs derived from the TX1-Unc and TX1-Cor lines formed aligned myofibers (*SI Appendix*, Fig. S7) but displayed distinct contractile phenotypes, with greater contraction stress generated by the corrected line (700 to 1,400 Pa) compared with the parental line (150 to 650 Pa) (Fig. 4 *O–R*). Furthermore, prednisolone treatment of the parental TX1-Unc line rescued force contraction to the level of the corrected TX1-Cor line (950 to 1,950 Pa) (Fig. 4 *O–Q* and *Movie S2*). These data demonstrate that DMD mutation leads to defects in force contraction in myofibers differentiated in vitro, and that these contractile defects can be largely rescued by prednisolone treatment.

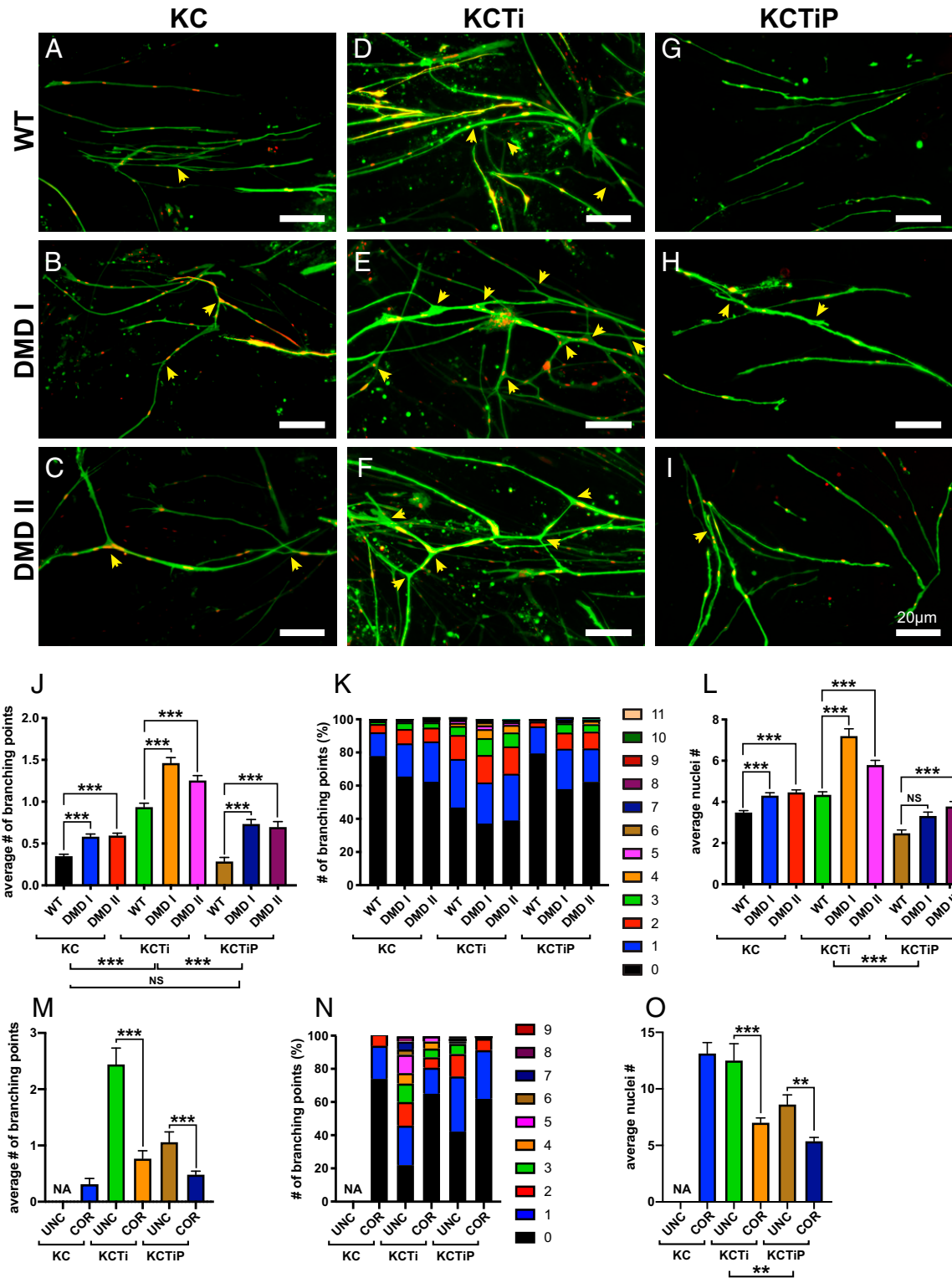


**Fig. 3.** Myofibers differentiated in vitro from dystrophin-deficient iPSC lines exhibit increased branching defects. (A–I) Isolated fibers from secondary cultures WT (A, D, and G), DMDI (B, E, and H), and DMDII (C, F, and I) iPSC lines labeled with membrane GFP (green) and mCherry (red) signals differentiated for 1 wk in KC (A–C), KCTi (D–F), or KCTiP (G–I) medium. Yellow arrowheads indicate branching points. (Scale bars: 20  $\mu$ m.) (J and K) Quantitative analysis of the number (#) of branching points in WT and DMD isogenic lines in the different culture media.  $***P < 0.0001$ , NS:  $P > 0.05$ . Bars show mean  $\pm$  SEM. (L) Quantitative analysis of the number of nuclei per fiber in WT and DMD isogenic lines in the different culture media.  $***P < 0.0001$ , NS:  $P > 0.05$ . Bars show mean  $\pm$  SEM. (M and N) Quantitative analysis of the number of branching points in TX1-Unc and TX1-Cor isogenic lines in the different culture media.  $***P < 0.0001$ . Bars show mean  $\pm$  SEM. No data are shown for TX1-Unc in KC medium (NA) as myogenic differentiation from these lines was poorly efficient in this condition. (O) Quantitative analysis of the number of nuclei per fiber in TX1-Unc and TX1-Cor isogenic lines in the different culture media.  $**P < 0.01$ ,  $***P < 0.0001$ . Bars show mean  $\pm$  SEM. Kruskal–Wallis nonparametric ANOVA test with planned multiple comparisons.

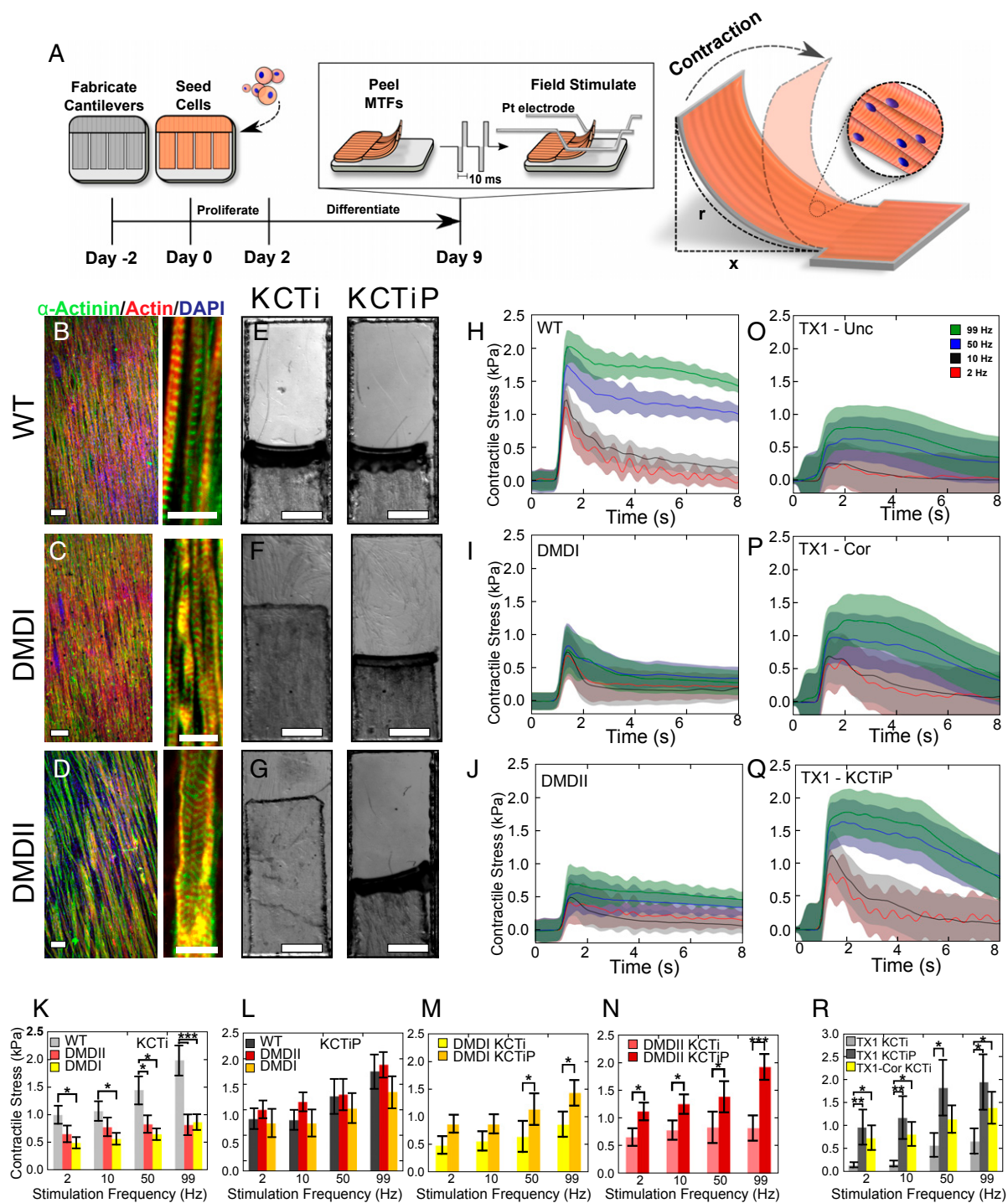


**Fig. 4.** Dystrophin mutant fibers derived in vitro exhibit contractile defects. (A) Experimental protocol and schematic illustration of MTF assay, for measuring contractile force. (B–D) Representative immunofluorescent micrograph of skeletal muscles grown on micromolded gelatin substrates, showing aligned confluent tissues (B) WT, (C) DMD I, and (D) DMD II (DAPI: blue, α-actinin: green, actin: red), with high-magnification inset showing sarcomere expression. (Scale bars: 100 μm Left, 10 μm Right.) (E–G) Bright-field micrographs of MTF cantilevers (top-down view) for WT (E), DMD I (F), and DMD II (G) myofibers cultured in KCTi (Left) and KCTiP (Right) media after stimulation (99 Hz), showing increased contraction in DMD cells after exposure to prednisolone. (Scale bars: 1 mm.) (H–J) Skeletal muscle contractile force as a function of stimulation time for WT (H), DMD I (I), and DMD II (J) mutant iPSC lines, demonstrating a positive force frequency relationship in the absence of dystrophin disruption (cells stimulated between 1.5 and 8 s at 2 to 99 Hz). (K–M) Comparison of peak contractile stresses generated by MTFs paced at 2 to 99 Hz. Showing a stronger contractile phenotype for WT cells (K) but a recovery of contractile phenotype in the presence of prednisolone treatment (KCTiP) (L–N). (n > 22; SI Appendix, Table S1; \*P < 0.05, \*\*P < 0.01, \*\*\*P < 0.001). (O–Q) Skeletal muscle contractile force as a function of stimulation time for DMD patient-derived cells (uncorrected in O and Q, corrected in P) in KCTi (O and P) and KCTiP (Q) media (cells were stimulated between 1.5 and 8 s at 2 to 99 Hz). (R) Peak contractile stress generated by patient derived cells paced at 2 to 99 Hz, showing a recovery of contractile phenotype for patient cells treated with prednisolone or corrected with CRISPR-Cas9. (n > 15; SI Appendix, Table S2). (Scale bars: 1 mm.) Pairwise t tests. All error bars given as the SEM.

**Dystrophin-Deficient Fibers Show Ca<sup>2+</sup> Hyperexcitability.** We next combined optogenetics and Ca<sup>2+</sup> imaging to study the dynamics of Ca<sup>2+</sup> handling in our DMD mutant myofibers differentiated in vitro. We used a lentivirus to infect proliferating myogenic precursors in SKGM, to express a blue-light sensitive channel-rhodopsin CheRiff (Fig. 5A) (30). After 7 to 10 d of differentiation in KCTi medium we incubated the myofiber cultures with the Ca<sup>2+</sup>-sensitive dye CaSiR-1 AM. We next mapped Ca<sup>2+</sup> responses across large (4 × 4 mm) cultures of myofibers using a custom-built ultrawide-field microscope (Fig. 5B and C). In all experiments, we observed a Ca<sup>2+</sup> “hyperexcitability” phenotype for myofibers lacking dystrophin, in which the amplitude of Ca<sup>2+</sup> responses was considerably higher for the mutant fibers than for healthy controls across the range of stimulus frequencies (Fig. 5D–F and Movie S3). For isogenic cultures, we observed statistically significant differences between WT and DMDII samples for all tested stimulus frequencies and between WT and DMDI samples for stimulus frequencies between 2 and 20 Hz (Fig. 5D). Notably, DMD fibers showed slower relaxation kinetics than did healthy fibers. The patient-derived line similarly showed statistically significant differences in Ca<sup>2+</sup> responses at each frequency tested (Fig. 5E and Movie S4), with greater Ca<sup>2+</sup> responses in the parental TX1-Unc line compared with the CRISPR-corrected TX1-Cor line. We further validated the patient-derived cell line results by repeating the experiment using a different Ca<sup>2+</sup>-sensitive dye (BioTrack 609) and by normalizing responses relative to an ionomycin treatment (Fig. 5F and Movie S5). This experiment again showed elevated Ca<sup>2+</sup> responses in dystrophin-deficient fibers, consistent with the Ca<sup>2+</sup> hyperexcitability phenotype. Each experiment was consistent with pathophysiological elevated and sensitized Ca<sup>2+</sup> responses in dystrophic fibers. Notably, observation of elevated “gain” of Ca<sup>2+</sup> signaling in response to a frequency ramp, as well as differences in relaxation kinetics, suggest an involvement of Ca<sup>2+</sup> handling feedbacks beyond an increase in leakage Ca<sup>2+</sup> currents across the plasma membrane. These results demonstrated that iPSC-derived skeletal myofibers can recapitulate phenotypes of Ca<sup>2+</sup> handling in both isogenic and patient derived cell lines.

## Discussion

Previous in vitro models based on myofibers differentiated from DMD patient iPSC lines have led to discordant results (15). A limitation of several of these studies is the comparison of iPSC lines from patients with lines from healthy subjects. The inherent variability in the differentiation potential of individual lines (31) is highly problematic as it can confound phenotypical studies. This problem can be circumvented by using isogenic lines in which a disease-causing mutation is introduced in a healthy parental line whose differentiation properties are well-characterized. Here, we report the engineering of human DMD mutant iPSC isogenic lines from a healthy WT line. We generated a deletion of exon 52 and a point mutation in exon 52 using CRISPR-Cas9 editing in the NCRM1 WT iPSC line. Thus, the phenotype of the engineered lines can be directly compared with the parental WT line whose myogenic differentiation has been well-characterized (17). We show that these two mutant lines exhibit largely similar phenotypes in all the assays tested but they nevertheless exhibit quantitative differences in most readouts. The reason for these differences is unclear but could be associated with differences in stability of the DMD mRNA generated in the two mutant backgrounds, leading to different amount of truncated dystrophin.

A second limitation from previously reported iPSC-based DMD models lies in the immature state of the myofibers generated in vitro using current myogenic differentiation protocols. Here, we describe a culture method which significantly increases myofiber maturation over existing protocols. While current strategies can result in differentiation of myogenic cells up to the embryonic-to-fetal transition (32, 33), our improved method results in well-organized myofibers with significant activation of the fast myosins IIx (*MYH1*),

IIa (*MYH2*), and IIb (*MYH4*), which are respectively first expressed during fetal, late fetal, and early postnatal stages (24). While most of DMD pathological landmarks have been defined during postnatal stages, the primary events leading to these defects likely happen during fetal development. The macroscopic architecture of fetal DMD muscles appears similar to normal fetal muscle, but myofiber defects and abnormal Ca<sup>2+</sup> signaling are already observed in DMD fetuses (34–36). Signs of degeneration and regeneration of the myofibers become conspicuous soon after birth, before clinically detectable symptoms (37). Studying these early stages of disease development is challenging due to the very limited access to DMD fetuses, and thus these early defects are poorly understood. Our system can therefore help understanding the earliest defects resulting from DMD absence in human patients.

In contrast to some studies (38, 39), we show that in our conditions the morphology and expression of myogenic markers of differentiating myogenic DMD-mutant iPSC lines appear largely similar to that of the WT parental NCRM1 line. The most striking morphological phenotype we observed in the differentiating DMD myofibers is abnormal branching, a defect which has been reported in muscle biopsies from boys with DMD and in myofibers of dystrophin-deficient *mdx* mice (6, 7, 40). The increased branching of DMD mutant myofibers observed in vitro was accompanied with an increased number of nuclei per fiber, suggesting increased fusion in DMD fibers. This supports the hypothesis that abnormal branching could result from increased fusion required by the sustained regeneration caused by myofiber death in DMD patients (6).

Using a tissue engineering approach in which myofibers are seeded on soft cantilevers (28) we observed a significant decrease in force contraction in the skeletal myofibers derived from DMD mutant iPSC lines compared with isogenic lines expressing dystrophin. Such a contraction defect has previously been observed in myofibers derived from patients’ primary myoblasts using the same platform (28). Such tissue-engineered models have been previously used to model cardiac disease including DMD (27, 41) and can provide several advantages when compared with in vivo models. First, the ability to use isogenic cell lines avoids potential changes in cellular contractility associated with differing genotypes, which can impact baseline muscle growth and tissue development (42). Second, this model can be used to directly test human-derived cells and subsequent pathophysiology, which have been difficult to recapitulate in animal models (43). Additionally, tissue-engineered models provide the capability of being used for personalized medicine applications, where potential therapeutic interventions are tested against a patient’s own cells. This is especially important in the case of DMD patients, where the dystrophin gene can be disrupted in one of several “hotspot” regions (44), meaning that individual patients may require distinct treatment regimes. Importantly, our observations demonstrate that human DMD mutant myofibers exhibit an intrinsic contraction defect as observed in zebrafish, mice, and dogs lacking dystrophin (8–10). Our in vitro system offers a unique opportunity to understand the cause of this defect and to search for therapeutic strategies to correct it.

The molecular mechanism through which dystrophin loss of function affects Ca<sup>2+</sup> signaling remains controversial. Here, we apply optogenetics to study Ca<sup>2+</sup> signaling in human DMD myofibers. We show that in vitro differentiation of skeletal myofibers can efficiently recapitulate the Ca<sup>2+</sup> hyperexcitability phenotype of dystrophin-deficient fibers. Our data are consistent with the Ca<sup>2+</sup> handling defects observed in differentiated fibers obtained by forced expression of MyoD in DMD patient iPSC in vitro (45). The hyperexcitability phenotype could result from disruption of the dystrophin–glycoprotein complex, leading to increased Ca<sup>2+</sup> leakage currents (46, 47). It is also possible that feedbacks involved in excitation–contraction coupling and Ca<sup>2+</sup>-induced Ca<sup>2+</sup> release are dysregulated in DMD myofibers. For example, the sarco/endoplasmic reticulum Ca<sup>2+</sup> ATPase (SERCA) has been reported to

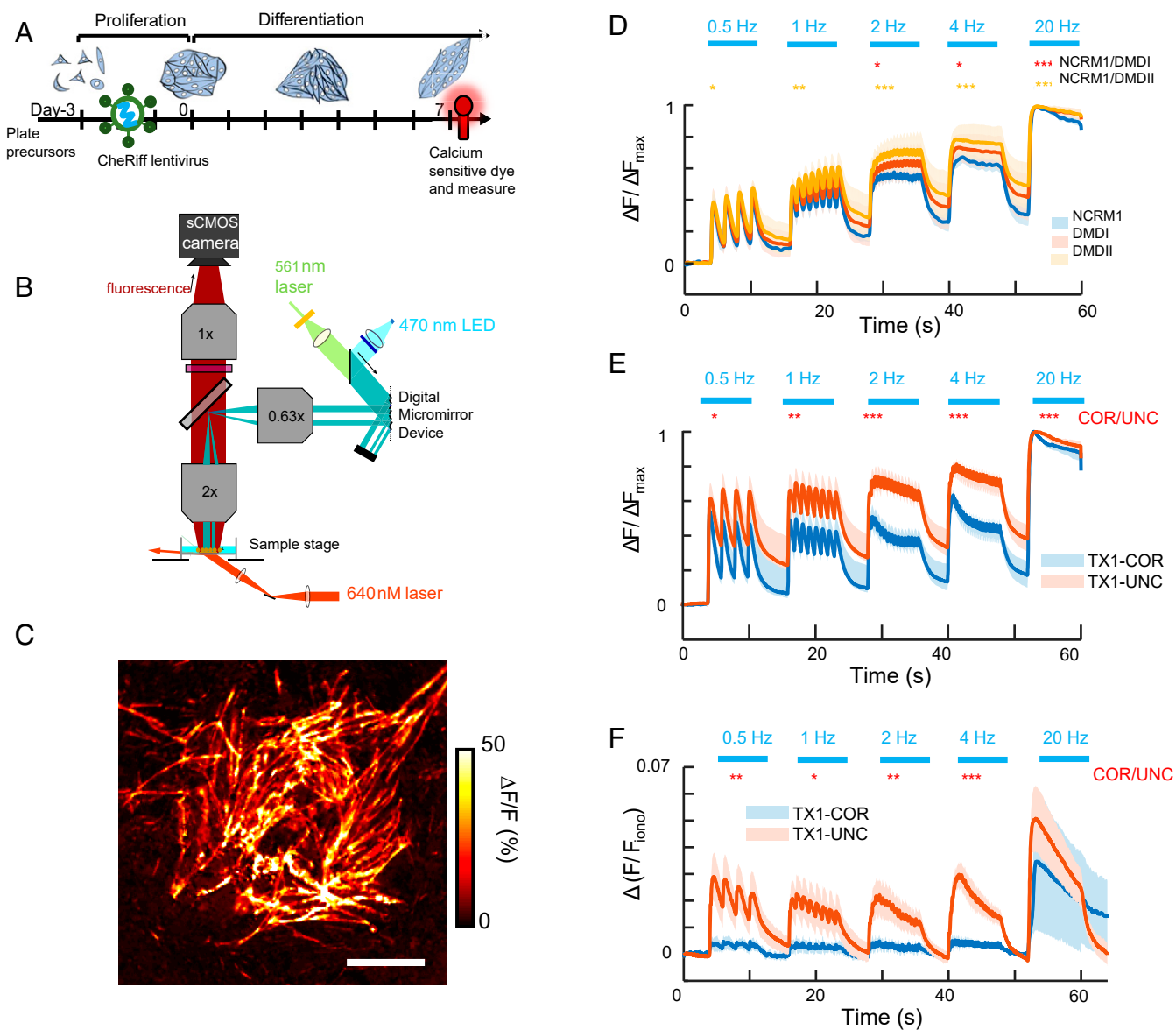


**Fig. 5.** All-optical profiling of Ca<sup>2+</sup> responses in healthy and dystrophic human iPSC myofibers. (A) Schematic of experimental timeline. Myocyte precursors are plated at low density in growth medium and inoculated with a lentiviral vector encoding CheRiff after 24 h. After 72 h, cells have reached confluence and are switched to differentiation media and cultured for seven additional days in KCT1 medium. After 7 d of differentiation, cultures are incubated with the Ca<sup>2+</sup>-sensitive dye CaSiR-1 AM and measured. (B) Diagram of optical setup. Red Ca<sup>2+</sup>-sensitive dyes are excited using oblique illumination, and Ca<sup>2+</sup>-sensitive fluorescence in the near infrared is collected with a high-numerical-aperture widefield objective. CheRiff stimulation is spatially targeted using a digital micromirror device. (C) Example image of blue-light-induced Ca<sup>2+</sup> response in a dish of iPSC cell-derived myocytes. (Scale bar: 1 mm.) (D) Profiling Ca<sup>2+</sup> response as a function of blue-light drive. Simultaneous differentiations of WT, DMDI, and DMDII cell lines (*n* = 6 dishes of each) were characterized via their Ca<sup>2+</sup> response to optogenetic stimulation across a range of drive frequencies (0.5 Hz to 20 Hz). Average traces reveal statistically significant differences between DMDI and NCRM1 (WT) lines (red asterisks) and between DMDII and NRCM1 (WT) lines (yellow asterisks). DMDI and DMDII lines showed no significant difference in Ca<sup>2+</sup> responses. (E) Same experiment as in *D*, but with parallel differentiations of a patient-derived iPSC line (TX1-Unc) and a corrected comparison (TX1-Cor) (*n* = 6 dishes of each). For patient-derived cells, *n* = 6 samples were analyzed for both TX1-Cor and TX1-Unc for the first replicate. (F) Replicate experiment comparing TX1-Cor and TX1-Unc patient-derived cultures, in which Ca<sup>2+</sup> signals are imaged with BioTracker 609 and normalized relative to responses to ionomycin application (10 μM). *n* = 4 samples were analyzed for each condition in the second replicate. Paired two-sample *t* tests. Confidence intervals of \**P* < 0.05, \*\**P* < 0.01, and \*\*\**P* < 0.001.

be dysregulated in DMD models, leading to a lack of Ca<sup>2+</sup> removal from the cytosol (48). This would be consistent with our observation of slower Ca<sup>2+</sup> relaxation kinetics after excitation in DMD lines. Thus, our work introduces a powerful system to study Ca<sup>2+</sup> handling in dystrophic myofibers.

Glucocorticoids are part of the standard of care for DMD patients in which they increase force and prolong ambulation (2). The mechanism of action of glucocorticoids underlying their beneficial

effect in patients has not been elucidated yet. The positive effect of glucocorticoids on patients is often attributed in part to their immunosuppressive properties (49, 50). One expected consequence of treatment is a decrease of inflammation associated with degeneration, leading to a slowing down of fibrosis progression and an improvement of muscle function. The glucocorticoid effects are paradoxical because these steroids can also trigger muscle atrophy (51). Prednisolone can also improve myofiber maturation in

primary myotubes cultured *in vitro*, suggesting that glucocorticoids might also act directly on muscle function (23, 52). In the *mdx* mouse and in patients, glucocorticoid treatment leads to metabolism reprogramming associated to improved performance of muscles (53). Here we demonstrate that Prednisolone can rescue the branching, fusion, and force contraction phenotypes in three different DMD mutant iPSC lines *in vitro*. Remarkably, an increase in force contraction is not observed when the parental WT lines are treated with prednisolone. Thus, our data suggest that prednisolone acts directly on the dystrophin-deficient myofibers to improve the pathological phenotype. Use of glucocorticoids is problematic in patients as it triggers significant side effects such as obesity or mood disorders (2). Our *in vitro* system provides an ideal platform to dissect the molecular action of glucocorticoids on myofibers. This will eventually enable the search for alternative therapies preserving the beneficial effect of glucocorticoids without the side effects.

## Materials and Methods

### iPSC Cell Maintenance and Differentiation.

**Maintenance.** Human iPSC cells were cultured as described previously (17, 40). Briefly, cells were cultured on Matrigel (BD Biosciences)-coated dishes in mTesR1 media (Stem Cell Technologies). Cells were passaged as aggregates or as single cells. The NCRM1 human iPSC line (RUCDR, Rutgers University) and its engineered derivatives were tested mycoplasma-free.

**Differentiation.** Serum-free myogenic primary differentiation of human iPSC clones was performed as described previously (17, 40). For secondary differentiation purposes, 3-wk-old primary myogenic cultures generated from iPSCs were dissociated as described and myogenic progenitors were replated at a density of 50 to 100,000/cm<sup>2</sup> onto Matrigel (354277; Corning)-coated dishes in skeletal muscle growth media (SKGM-2, CC-3245; Lonza) with 10  $\mu$ M ROCK inhibitor (1254; R&D Systems) (17). After 24 h, medium was changed to SKGM-2 media without ROCK inhibitor. Cultures were allowed to proliferate for 1 to 2 d, at which point they reached ~90% confluence. Cultures were then induced for myogenic differentiation with DMEM/F12 supplemented with 2% knock-out serum replacement (10828028; Invitrogen), 1  $\mu$ M Chiron (4423; Tocris), 0.2% Pen/Strep (15140122; Life Technologies), and 1 $\times$  ITS (41400045; Life Technologies), with or without 10  $\mu$ M of the TGF- $\beta$  inhibitor SB431542 (1614; Tocris) (KCTi) or 10  $\mu$ M of prednisolone (P6004; Sigma-Aldrich) (KCTiP). Following induction, differentiation medium was changed on days 1 and 2 and then was refreshed every other day for 1 wk.

**Generation of Isogenic DMD Mutant Cell Lines.** To generate the DMD cell line lacking exon 52 (DMDI), NCRM1 cells were transfected using two pSpCas9 (BB)-2A-GFP plasmids: one containing a guide targeting the 5' intron flanking the exon 52 of the DMD gene and one containing a guide targeting the 3' intron flanking the exon 52 (*SI Appendix, Table S3*) (25). To generate the DMD cell line exhibiting a stop codon within exon 52 (DMDII), NCRM1 cells were transfected using a pSpCas9 (BB)-2A-GFP containing a guide targeting exon 52 and a single stranded oligodeoxynucleotide (Integrated DNA Technologies) containing the mutated region (*SI Appendix, Table S3*). Transfected GFP-positive single cells were cultured clonally. For DMDI, screening was performed by PCR using primers flanking the deleted region (*SI Appendix, Table S3*). Clones exhibiting a perfect repair by nonhomologous end joining were selected after sequencing and named DMDI. For DMDII, positive clones were screened by PCR using the *SacI* restriction enzyme and, after sequencing, clones exhibiting perfect homology directed repair were selected and named DMDII. Detailed methodology is described in *SI Appendix*.

### Bulk RNA-Seq Analysis.

**Sample preparation and RNA extraction.** The NCRM1 line was differentiated into myogenic cultures as described in ref. 17 and cells were harvested on days 0, 8, 16, 24, and 32 of differentiation. For secondary differentiation, primary cultures were dissociated at day 21 and replated as described above in SKGM. Samples were collected after 2 d in SKGM (SKGM-2, CC-3245; Lonza) culture. The cultures were further differentiated in three different conditions: KC, KCTi, and KCTiP. For each condition, cells were harvested after 7 and 15 d of differentiation. For each time point samples were collected from three independent experiments. To compare the isogenic DMD and the parental iPSC lines, cells were differentiated into myogenic cultures and replated for secondary differentiation as described above. Cells were

cultured in SKGM medium for 2 d followed by culture in KC differentiation medium for 1 wk. RNA was isolated using a NucleoSpin RNA kit (740955; Macherey and Nagel) following the manufacturer's protocol. RNA libraries were prepared using Roche Kapa mRNA Hyper Prep and sequencing was performed on Illumina NextSeq. 500 sequencing platform.

**Bulk RNA sequencing data analysis.** For both experiments, we used STAR (v2.5.1b) (54) to map sequenced reads to the human reference genome (GRCh38 release 77 from ENSEMBL). Gene counts were then quantified, from mapped reads, using featureCounts (1.6.2) (55). Starting from the raw gene counts, normalization and differential expression analysis were then performed using DESeq2 (v 1.22.2) (56). Genes were defined as differentially expressed when the absolute fold-change value was greater than 2 and the false discovery rate lower than 0.01. GO enrichment analysis was performed on the differentially expressed genes using EnrichR (57) and AnnoMiner (58). To produce heat maps for genes of interest from the muscle differentiation assays, we first normalized read counts and calculated the rlog using DESeq2. To calculate up- or down-regulation, we computed the log difference of the average of the triplicates against the baseline value (average over all conditions) for each gene. All data generated in this study were submitted to Gene Expression Omnibus (accession no. GSE164874).

**Western Blot Analysis.** Western blot analysis for human iPSC-derived muscles was performed using antibodies to dystrophin (DYS1-CE; Leica) and tubulin (MAB1864; Millipore). Goat anti-mouse and goat anti-rat horseradish peroxidase-conjugated secondary antibodies were used for described experiments.

**Immunohistochemistry.** Primary myogenic cultures were generated as described above. For secondary cultures, cells were replated on Matrigel (354277; Corning)-coated glass-bottom plates at a density of 50,000 to 100,000 cells/cm<sup>2</sup>. Cells were replated in SKGM medium (SKGM-2, CC-3245; Lonza) supplemented with Rock inhibitor (1254; R&D Systems). The next day, medium was replaced by fresh SKGM. Cells were then differentiated in KC/KCTi/KCTiP medium and cell cultures were fixed for 20 min in 4% paraformaldehyde (15710; Electron Microscopy Sciences) at room temperature. Cultures were rinsed three times in phosphate-buffered saline (PBS), followed by blocking buffer composed of PBS supplemented with 3% heat-inactivated donkey serum (017-000-121; Jackson Immuno Research) and 0.1% Triton X-100 (T8787; Sigma-Aldrich). Primary antibodies were then diluted in blocking buffer and incubated overnight at 4  $^{\circ}$ C. Cultures were then washed three times with PBS and incubated with secondary antibodies (donkey anti-mouse/rabbit IgG H+L Alexa Fluor cross-adsorbed secondary antibody, 1:500) and Hoechst (5  $\mu$ g/mL) in blocking buffer for 1 h at room temperature. Cultures were then washed and stored in PBS until analyzed. Images were captured using a Zeiss LSM780 confocal microscope using 10 $\times$  and 20 $\times$  objectives. Images were analyzed using Fiji (59). For quantification of MYOG- and PAX7-positive cells in myogenic culture, cells were cultured in SKGM for 2 d following the standard secondary differentiation protocol. After immunostaining, cells were imaged using InCell 2000 arrayscan imaging platform (GE Life Sciences) and the number of MYOG- and PAX7-stained cells was quantified using Fiji (59). Averages and significance were statistically analyzed using a paired *t* test using Prism software. Primary antibodies used in this study are listed in *SI Appendix, Table S4*.

**Reverse Transcription qPCR.** Primary myogenic cultures were generated as described above. For secondary cultures, cells were replated on Matrigel (354277; Corning)-coated plastic-bottom plates at a density of 50,000 to 100,000 cells/cm<sup>2</sup>. Cells were replated in SKGM medium (SKGM-2, CC-3245; Lonza) supplemented with Rock inhibitor (1254; R&D Systems). The next day, medium was replaced by fresh SKGM. Cells were then differentiated in KC/KCTi/KCTiP medium for 7 d. Samples were collected from three independent experiments. RNA was isolated using NucleoSpin RNA kit (740955; Macherey and Nagel) following the manufacturer's protocol. Reverse transcription of RNA into complementary DNA (cDNA) was done using iScript cDNA Synthesis Kit (1708890; Bio-Rad). cDNA quantification was obtained by real-time qPCR (LightCycler 480; Roche) using iTaQ Universal SYBR Green Supermix (172-5124; Bio-Rad) according to the manufacturer's instructions. RPL37A transcript levels were used as a reference for the normalization of each target within each sample. Fold change of mRNA expression ( $2^{-\Delta\Delta Ct}$ ) was calculated in reference to KCTiP condition. Significance was statistically analyzed using a paired *t* test (Prism 8 software; GraphPad). Primers used for this study are listed in *SI Appendix, Table S5*.

**Electron Microscopy.** Myogenic progenitors were replated in SKGM for 2 d and then differentiated in KC/KCTi/KCTiP medium for 10 d. Samples were then fixed, followed by osmication and uranyl acetate staining, dehydration in

graded alcohols, and embedding in Taab 812 Resin (Marivac Ltd.). Eighty-nanometer sections were cut using the Leica Ultracut 5 microtome, placed on carbon-coated slot Cu grids, stained with 0.2% lead citrate, and then viewed and imaged with the JEOL 1,200× electron microscope. Detailed methods are described in *SI Appendix*.

**Fiber Branching Quantification.** Myogenic progenitors were replated in SKGM-2 medium. Twenty-four hours later, cells were transfected with Tol2 CAGGS-nls mCherry IRES GFPcaax and CAGGS transposase (kindly donated by C. Marcelle, Australian Regenerative Medicine Institute, Clayton, VIC, Australia). Cells were transfected with the plasmids using Lipofectamine 3000 (Thermo Fisher) at standard concentrations as suggested in the manufacturer's protocols. Cells were allowed to recover 24 h after lipofectamine, meaning differentiation was induced 48 h after replating. One day after transfection, cells were induced for differentiation using KC, KCTi, or KCTIP media for 7 d. Plates were then fixed and immunostained for GFP (ab13970; Abcam) and red fluorescent protein (ab62341; Abcam) and MF20 (DSHB) and the entire wells were imaged using the InCell 2000 arrayscan imaging platform (GE Life Sciences). Detailed methods are described in *SI Appendix*.

**Contractility/Force Measurements.** Gelatin MTF chips were manufactured as previously reported (60). Myogenic progenitors were generated and replated on patterned gelatin MTFs in SKGM medium. Cells were then differentiated over 1-wk period in KCTi or KCTIP media. After 1 wk of differentiation MTF experiments were performed. Video micrographs were recorded on a Zeiss Discovery.V12 stereomicroscope. Contractile stress was calculated using a custom Python script. Detailed methods are described in *SI Appendix*.

**Calcium Signaling Analysis.** Myogenic progenitors were replated at low density in SKGM and incubated with low-titer lentivirus encoding CheRiff-CFP. Cultures were induced for myogenic differentiation in KCTi medium for 10 d. CheRiff-expressing myocyte cultures were stained either with CaSiR-1

AM (Goryo Chemical) or BioTracker 609 AM Red Ca<sup>2+</sup> Dye (EMD Millipore). A loading solution was prepared by diluting calcium dye stocks to 2 μM concentration in the presence of 0.02% final concentration of Pluronic F127 (Sigma). Myofiber samples were stained in loading solution, washed twice in PBS to remove residual dye, and then transferred to Tyrode's solution. Calcium imaging, measurement, and data analysis were performed as described in *SI Appendix* (61).

**Data Availability.** RNA-seq data have been deposited in Gene Expression Omnibus (accession no. [GSE164874](https://www.ncbi.nlm.nih.gov/geo/query/acc.cgi?acc=GSE164874)).

**ACKNOWLEDGMENTS.** We thank Lou Kunkel, Emanuela Gussoni, and Felipe Leite for critical reading of the manuscript and Suvi Avio for technical help in the early stages of the project. We thank the NeuroTechnology Studio at Brigham and Women's Hospital for providing InCell instrument access and consultation on data acquisition and data analysis. This work was supported by a strategic grant (17099) from the French Muscular Dystrophy Association (AFM), by an advanced grant (FP7-IDEAS-ERC-249931) from the European Research Council, by the FP7 EU grant Plurimes (602423), and by a Human Frontier Science Program award (RGP0052/2018) to O.P. and by an AFM postdoctoral grant (20581) to D.S. Additionally, this work was sponsored in part by the John A. Paulson School of Engineering and Applied Sciences at Harvard University, the Wyss Institute for Biologically Inspired Engineering at Harvard University, and Harvard Materials Research Science and Engineering Center grant DMR-1420570 to K.K.P. and an NIH Organ Design and Engineering postdoctoral training fellowship under T32EB016652 to J.F.Z., H.M.M., and A.E.C. were supported by the Howard Hughes Medical Institute. This work was supported in part by the Senator Paul D. Wellstone Muscular Dystrophy Specialized Research Center at University of Texas Southwestern Medical Center grant (HD087351) to E.N.O. B.H. and F.M. are supported by Agence Nationale de la Recherche (ANR) grant ANR-18-CE45-0016. This work was supported by the "la Caixa" Foundation (ID 100010434) under agreement LCF/BQ/AA18/11680032 to A.R.-d.I.R.

1. F. Rahimov, L. M. Kunkel, The cell biology of disease: Cellular and molecular mechanisms underlying muscular dystrophy. *J. Cell Biol.* **201**, 499–510 (2013).
2. E. Mattheus, R. Brassington, T. Kuntzer, F. Jichi, A. Y. Manzur, Corticosteroids for the treatment of Duchenne muscular dystrophy. *Cochrane Database Syst. Rev.* **2016**, CD003725 (2016).
3. B. J. Petrof, J. B. Shrager, H. H. Stedman, A. M. Kelly, H. L. Sweeney, Dystrophin protects the sarcolemma from stresses developed during muscle contraction. *Proc. Natl. Acad. Sci. U.S.A.* **90**, 3710–3714 (1993).
4. A. R. Burr, J. D. Molkenin, Genetic evidence in the mouse solidifies the calcium hypothesis of myofiber death in muscular dystrophy. *Cell Death Differ.* **22**, 1402–1412 (2015).
5. J. E. Brenman, D. S. Chao, H. Xia, K. Aldape, D. S. Bredt, Nitric oxide synthase complexed with dystrophin and absent from skeletal muscle sarcolemma in Duchenne muscular dystrophy. *Cell* **82**, 743–752 (1995).
6. S. Chan, S. I. Head, The role of branched fibres in the pathogenesis of Duchenne muscular dystrophy. *Exp. Physiol.* **96**, 564–571 (2011).
7. H. Schmalbruch, Regenerated muscle fibers in Duchenne muscular dystrophy: A serial section study. *Neurology* **34**, 60–65 (1984).
8. J. J. Widrick *et al.*, Muscle dysfunction in a zebrafish model of Duchenne muscular dystrophy. *Physiol. Genomics* **48**, 850–860 (2016).
9. D. A. Lowe, B. O. Williams, D. D. Thomas, R. W. Grange, Molecular and cellular contractile dysfunction of dystrophic muscle from young mice. *Muscle Nerve* **34**, 92–100 (2006).
10. H. T. Yang *et al.*, Dystrophin deficiency compromises force production of the extensor carpi ulnaris muscle in the canine model of Duchenne muscular dystrophy. *PLoS One* **7**, e44438 (2012).
11. R. H. Fink, D. G. Stephenson, D. A. Williams, Physiological properties of skinned fibres from normal and dystrophic (Duchenne) human muscle activated by Ca<sup>2+</sup> and Sr<sup>2+</sup>. *J. Physiol.* **420**, 337–353 (1990).
12. T. A. Partridge, The mdx mouse model as a surrogate for Duchenne muscular dystrophy. *FEBS J.* **280**, 4177–4186 (2013).
13. D. Merrick, L. K. Stadler, D. Larner, J. Smith, Muscular dystrophy begins early in embryonic development deriving from stem cell loss and disrupted skeletal muscle formation. *Dis. Model. Mech.* **2**, 374–388 (2009).
14. J. Chal, O. Pourquie, Making muscle: Skeletal myogenesis in vivo and in vitro. *Development* **144**, 2104–2122 (2017).
15. D. Piga *et al.*, Human induced pluripotent stem cell models for the study and treatment of Duchenne and Becker muscular dystrophies. *Ther. Adv. Neurol. Disord.* **12**, 1756286419833478 (2019).
16. M. Diaz-Cuadros *et al.*, In vitro characterization of the human segmentation clock. *Nature* **580**, 113–118 (2020).
17. J. Chal *et al.*, Generation of human muscle fibers and satellite-like cells from human pluripotent stem cells in vitro. *Nat. Protoc.* **11**, 1833–1850 (2016).
18. Z. Al Tanoury, J. Rao, F. Marchiano, B. Habermann, O. Pourquie, Prednisolone rescues Duchenne Muscular Dystrophy phenotypes in human pluripotent stem cells-derived skeletal muscle in vitro. *Gene Expression Omnibus*. <https://www.ncbi.nlm.nih.gov/geo/query/acc.cgi?acc=GSE164874>. Deposited 14 January 2021.
19. G. Messina *et al.*, Nfix regulates fetal-specific transcription in developing skeletal muscle. *Cell* **140**, 554–566 (2010).
20. M. R. Hicks *et al.*, ERBB3 and NGFR mark a distinct skeletal muscle progenitor cell in human development and hPSCs. *Nat. Cell Biol.* **20**, 46–57 (2018).
21. J. Melendez *et al.*, TGFβ signalling acts as a molecular brake of myoblast fusion. *Nat. Commun.* **12**, 749 (2021).
22. J. T. Busada, J. A. Cidlowski, Mechanisms of glucocorticoid action during development. *Curr. Top. Dev. Biol.* **125**, 147–170 (2017).
23. S. Braun *et al.*, Stimulating effects of prednisolone on acetylcholine receptor expression and myogenesis in primary culture of newborn rat muscle cells. *J. Neurol. Sci.* **92**, 119–131 (1989).
24. S. Schiaffino, A. C. Rossi, V. Smerdu, L. A. Leinwand, C. Reggiani, Developmental myosins: Expression patterns and functional significance. *Skelet. Muscle* **5**, 22 (2015).
25. F. A. Ran *et al.*, Genome engineering using the CRISPR-Cas9 system. *Nat. Protoc.* **8**, 2281–2308 (2013).
26. N. Janghra *et al.*, Correlation of utrophin levels with the dystrophin protein complex and muscle fibre regeneration in Duchenne and Becker muscular dystrophy muscle biopsies. *PLoS One* **11**, e0150818 (2016).
27. C. Long *et al.*, Correction of diverse muscular dystrophy mutations in human engineered heart muscle by single-site genome editing. *Sci. Adv.* **4**, eaap9004 (2018).
28. A. P. Nesmith *et al.*, A human in vitro model of Duchenne muscular dystrophy muscle formation and contractility. *J. Cell Biol.* **215**, 47–56 (2016).
29. C. N. Maganaris, V. Baltzopoulos, D. Ball, A. J. Sargeant, In vivo specific tension of human skeletal muscle. *J. Appl. Physiol.* (1985) **90**, 865–872 (2001).
30. D. R. Hochbaum *et al.*, All-optical electrophysiology in mammalian neurons using engineered microbial rhodopsins. *Nat. Methods* **11**, 825–833 (2014).
31. K. Osafune *et al.*, Marked differences in differentiation propensity among human embryonic stem cell lines. *Nat. Biotechnol.* **26**, 313–315 (2008).
32. H. Xi *et al.*, A human skeletal muscle atlas identifies the trajectories of stem and progenitor cells across development and from human pluripotent stem cells. *Cell Stem Cell* **27**, 158–176.e10 (2020).
33. Z. Al Tanoury *et al.*, Differentiation of the human PAX7-positive myogenic precursors/satellite cell lineage in vitro. *Development* **47**, dev187344 (2020).
34. A. E. Emery, Muscle histology and creatine kinase levels in the foetus in Duchenne muscular dystrophy. *Nature* **266**, 472–473 (1977).
35. A. E. Emery *et al.*, Antenatal diagnosis of Duchenne muscular dystrophy. *Lancet* **1**, 847–849 (1979).
36. A. Farini *et al.*, Inositol 1,4,5-trisphosphate (IP3)-dependent Ca<sup>2+</sup> signaling mediates delayed myogenesis in Duchenne muscular dystrophy fetal muscle. *Development* **143**, 658–669 (2016).
37. C. M. Pearson, Histopathological features of muscle in the preclinical stages of muscular dystrophy. *Brain* **85**, 109–120 (1962).
38. I. Y. Choi *et al.*, Concordant but varied phenotypes among Duchenne muscular dystrophy patient-specific myoblasts derived using a human iPSC-based model. *Cell Rep.* **15**, 2301–2312 (2016).

39. A. Moretti *et al.*, Somatic gene editing ameliorates skeletal and cardiac muscle failure in pig and human models of Duchenne muscular dystrophy. *Nat. Med.* **26**, 207–214 (2020).
40. J. Chal *et al.*, Differentiation of pluripotent stem cells to muscle fiber to model Duchenne muscular dystrophy. *Nat. Biotechnol.* **33**, 962–969 (2015).
41. G. Wang *et al.*, Modeling the mitochondrial cardiomyopathy of Barth syndrome with induced pluripotent stem cell and heart-on-chip technologies. *Nat. Med.* **20**, 616–623 (2014).
42. P. B. Costa *et al.*, Effects of static stretching on the hamstrings-to-quadriceps ratio and electromyographic amplitude in men. *J. Sports Med. Phys. Fitness* **49**, 401–409 (2009).
43. J. W. McGreevy, C. H. Hakim, M. A. McIntosh, D. Duan, Animal models of Duchenne muscular dystrophy: From basic mechanisms to gene therapy. *Dis. Model. Mech.* **8**, 195–213 (2015).
44. G. Esposito *et al.*, Precise mapping of 17 deletion breakpoints within the central hotspot deletion region (introns 50 and 51) of the DMD gene. *J. Hum. Genet.* **62**, 1057–1063 (2017).
45. E. Shoji *et al.*, Early pathogenesis of Duchenne muscular dystrophy modelled in patient-derived human induced pluripotent stem cells. *Sci. Rep.* **5**, 12831 (2015).
46. P. Y. Fong, P. R. Turner, W. F. Denetclaw, R. A. Steinhardt, Increased activity of calcium leak channels in myotubes of Duchenne human and mdx mouse origin. *Science* **250**, 673–676 (1990).
47. A. Franco Jr, J. B. Lansman, Calcium entry through stretch-inactivated ion channels in mdx myotubes. *Nature* **344**, 670–673 (1990).
48. A. Voit *et al.*, Reducing sarcolipin expression mitigates Duchenne muscular dystrophy and associated cardiomyopathy in mice. *Nat. Commun.* **8**, 1068 (2017).
49. J. T. Kissel, K. L. Burrow, K. W. Rammohan, J. R. Mendell; CIDD Study Group, Mononuclear cell analysis of muscle biopsies in prednisone-treated and untreated Duchenne muscular dystrophy. *Neurology* **41**, 667–672 (1991).
50. M. Wehling-Henricks, J. J. Lee, J. G. Tidball, Prednisolone decreases cellular adhesion molecules required for inflammatory cell infiltration in dystrophin-deficient skeletal muscle. *Neuromuscul. Disord.* **14**, 483–490 (2004).
51. F. Kanda *et al.*, Steroid myopathy: Pathogenesis and effects of growth hormone and insulin-like growth factor-I administration. *Horm. Res.* **56** (suppl. 1), 24–28 (2001).
52. R. M. Sklar, R. H. Brown Jr, Methylprednisolone increases dystrophin levels by inhibiting myotube death during myogenesis of normal human muscle in vitro. *J. Neurol. Sci.* **101**, 73–81 (1991).
53. M. Quattrocchi *et al.*, Pulsed glucocorticoids enhance dystrophic muscle performance through epigenetic-metabolic reprogramming. *JCI Insight* **4**, e132402 (2019).
54. A. Dobin *et al.*, STAR: Ultrafast universal RNA-seq aligner. *Bioinformatics* **29**, 15–21 (2013).
55. Y. Liao, G. K. Smyth, W. Shi, featureCounts: An efficient general purpose program for assigning sequence reads to genomic features. *Bioinformatics* **30**, 923–930 (2014).
56. M. I. Love, W. Huber, S. Anders, Moderated estimation of fold change and dispersion for RNA-seq data with DESeq2. *Genome Biol.* **15**, 550 (2014).
57. M. V. Kuleshov *et al.*, Enrichr: A comprehensive gene set enrichment analysis web server 2016 update. *Nucleic Acids Res.* **44** (W1), W90–W97 (2016).
58. M. Meiler, F. Marchiano, M. V. Weikunat, F. Schnorrer, B. H. Habermann, AnnoMiner: A new web-tool to integrate epigenetics, transcription factor occupancy and transcriptomics data to predict transcriptional regulators. *bioRxiv* [Preprint] (2021). <https://www.biorxiv.org/content/10.1101/2021.01.28.428613v1> (Accessed 28 January 2021).
59. J. Schindelin *et al.*, Fiji: An open-source platform for biological-image analysis. *Nat. Methods* **9**, 676–682 (2012).
60. M. L. McCain, A. Agarwal, H. W. Nesmith, A. P. Nesmith, K. K. Parker, Micromolded gelatin hydrogels for extended culture of engineered cardiac tissues. *Biomaterials* **35**, 5462–5471 (2014).
61. C. A. Werley, M. P. Chien, A. E. Cohen, Ultrawidefield microscope for high-speed fluorescence imaging and targeted optogenetic stimulation. *Biomed. Opt. Express* **8**, 5794–5813 (2017).